


FULL PAPER

Open Access



Severe L-band scintillation over low-to-mid latitudes caused by an extreme equatorial plasma bubble: joint observations from ground-based monitors and GOLD

Jonas Sousasantos^{1*} , Josemaria Gomez Socola¹ , Fabiano S. Rodrigues¹ , Richard W. Eastes² , Christiano G. M. Brum³  and Pedrina Terra³ 

Abstract

The occurrence of plasma irregularities and ionospheric scintillation over the Caribbean region have been reported in previous studies, but a better understanding of the source and conditions leading to these events is still needed. In December 2021, three ground-based ionospheric scintillation and Total Electron Content monitors were installed at different locations over Puerto Rico to better understand the occurrence of ionospheric irregularities in the region and to quantify their impact on transionospheric signals. Here, the findings for an event that occurred on March 13–14, 2022 are reported. The measurements made by the ground-based instrumentation indicated that ionospheric irregularities and scintillation originated at low latitudes and propagated, subsequently, to mid-latitudes. Imaging of the ionospheric F-region over a wide range of latitudes provided by the GOLD mission confirmed, unequivocally, that the observed irregularities and the scintillation were indeed caused by extreme equatorial plasma bubbles, that is, bubbles that reach abnormally high apex heights. The joint ground- and space-based observations show that plasma bubbles reached apex heights exceeding 2600 km and magnetic dip latitudes beyond 28°. In addition to the identification of extreme plasma bubbles as the source of the ionospheric perturbations over low-to-mid latitudes, GOLD observations also provided experimental evidence of the background ionospheric conditions leading to the abnormally high rise of the plasma bubbles and to severe L-band scintillation. These conditions are in good agreement with the theoretical hypothesis previously proposed.

Keywords Extreme Plasma Bubbles, Severe L-band scintillation, Low-to-mid latitude irregularities, Space weather

*Correspondence:

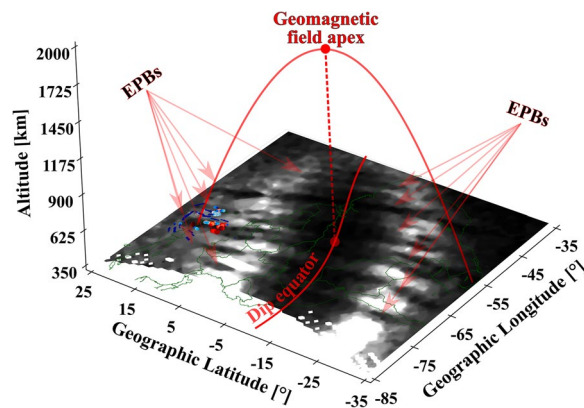
Jonas Sousasantos
jonas.ssts@utdallas.edu

Full list of author information is available at the end of the article



© The Author(s) 2023. **Open Access** This article is licensed under a Creative Commons Attribution 4.0 International License, which permits use, sharing, adaptation, distribution and reproduction in any medium or format, as long as you give appropriate credit to the original author(s) and the source, provide a link to the Creative Commons licence, and indicate if changes were made. The images or other third party material in this article are included in the article's Creative Commons licence, unless indicated otherwise in a credit line to the material. If material is not included in the article's Creative Commons licence and your intended use is not permitted by statutory regulation or exceeds the permitted use, you will need to obtain permission directly from the copyright holder. To view a copy of this licence, visit <http://creativecommons.org/licenses/by/4.0/>.

Graphical Abstract



Introduction

Depletions in the ionospheric Total Electron Content (TEC) and intense radio scintillation are known to occur often over low latitudes (Basu et al. 1976; 1988; Beach and Kintner 2001). It has been shown that these low-latitude TEC depletions are caused by Equatorial Plasma Bubbles (EPBs), which are large-scale (> 10 s of km) manifestations of the Generalized Rayleigh–Taylor instability (GRTi). The GRTi finds favorable growth conditions in the equatorial F-region near sunset hours (Woodman and La Hoz 1976). Scintillation is the result of the diffraction of transionospheric radio waves caused by smaller scale irregularities (100 s of meters to a few km) generated by secondary instabilities within the EPBs (Haerendel et al. 1992). EPBs are known to occur frequently, particularly during equinoxes and summer solstices (Sobral et al. 2002), in most longitude sectors, and the scintillation associated with EPBs is known to be the most intense in the globe (Jiao and Morton 2015; Juan et al. 2018). It is also known that EPBs are field-aligned ionospheric density depletions and, therefore, as they rise over the magnetic equator, they also extend to increasingly higher magnetic latitudes. As a consequence, an EPB reaching high apex altitudes over the equator may extend to latitudes far from the equatorial region. Current research seeks a better understanding of the occurrence of these extreme EPBs and the underlying ionospheric conditions leading to these events. Here the nomenclature extreme EPBs refers to EPBs reaching apex altitudes ≥ 2000 km.

EPB research is also motivated by their impact, through scintillation, on various radio systems used for communication, navigation, and remote sensing (Kelly et al. 2014; Moraes et al. 2018; Fernandez et al. 2020; Portella et al.

2021; Carrano et al. 2021; Salles et al. 2021; Sousasantos et al. 2022). These factors have led to the deployment of various observing platforms and routine ionospheric observations at low latitudes. The mid-latitude ionosphere, however, has been thought to be devoid of significant disturbances and threats to radio systems. That led to a reduced number of instrument deployments and observations at mid-latitudes. Notable exceptions were observations made by the Incoherent Scatter Radar (ISR) of the Arecibo Observatory in Puerto Rico (PR). While the observations made by the Arecibo ISR were limited in number and focused on the quiescent ionosphere, they served to provide evidence of the occurrence of ionospheric disturbances that departed significantly from expectations for the mid-latitude region (Mathews et al. 2001a, 2001b). In some cases, observations made by the Arecibo ISR were combined with simultaneous airglow, TEC, or coherent scatter radar measurements to confirm the occurrence of large-scale ionospheric disturbances and smaller scale irregularities (Martinis and Mendillo 2007; Martinis et al. 2009). In most cases, the ionospheric disturbances detected near Arecibo were attributed to Medium-Scale Traveling Ionospheric Disturbances—MSTIDs (Martinis et al. 2010).

Martinis and Mendillo (2007), however, reported the unusual case of airglow depletions over Arecibo that were attributed to an extreme EPB reaching mid-latitudes (apex heights above 2200 km). While airglow measurements are difficult to make, given the requirements of sky conditions, Martinis and Mendillo (2007) were still able to report airglow measurements made in El Leoncito, Argentina, slightly west of the conjugate point of Arecibo in the southern hemisphere, providing convincing

observational evidence to support their hypothesis of an extreme EPB as the source of the ionospheric disturbance observed over Arecibo. The equatorial region, however, was not covered by their experiment.

Previous studies using coherent backscatter radar over the Peruvian equatorial region indicated that extreme EPBs are rare events. Chapagain et al. (2009) used 10 years (1996–2006) of radar measurements to investigate the behavior of the maximum height of EPBs (radar plumes) over the equator (Jicamarca) as a function of solar flux conditions. They found that the maximum height of the plumes does increase with F10.7, but few plumes reached 1600 km apex heights. In their data set, they did not find plumes reaching apex heights greater than 1800 km. Notwithstanding, an increasing number of works reported the occurrence of possible extreme EPBs using data from ion density measurements made by instruments boarded in satellites (Basu et al. 2005, 2007; Huang et al. 2007a); from the Global Navigation Satellite System (GNSS) ground receiver networks (Ma and Maruyama 2006; Cherniak and Zakharenkova 2016, 2022; Katamzi-Joseph et al. 2017; Li et al. 2018; Aa et al. 2018; Zakharenkova and Cherniak 2020, 2021; Sori et al. 2022), and all-sky imagers (Martinis et al. 2015). Recently, Rodrigues et al. (2021) reported the occurrence of mid-latitude scintillation and TEC depletions over Southern US (43.2°N magnetic dip latitude) that could have been associated with an extreme EPB as hypothesized by Martinis et al. (2015) or by a super Medium-Scale Traveling Ionospheric Disturbance (MSTID) as proposed by Kil et al. (2016). Also, during unusual events, such as the Hunga Tonga-Hunga Ha'apai volcano eruption, strong ionospheric irregularities over latitudes far away from the geomagnetic equator have been reported (Aa et al. 2022; Rajesh et al. 2022). These results indicate the need of joint space-and-ground-based observations for unequivocal determination of the sources of irregularities and scintillation over mid-latitudes.

This work presents results related to observations made by a new set of ground-based instruments contributing to a better understanding of the occurrence and impact of ionospheric disturbances observed at mid-latitudes. These observations were complemented with images from the Global-scale Observations of the Limb and

Disk (GOLD) mission allowing the determination of the source of the ionospheric disturbances reaching dip latitudes > 28°. More specifically, new observations of TEC depletions and severe amplitude scintillations reaching the latitude of Puerto Rico and above are reported. The spatial and temporal behavior of scintillation provided by the ground-based observations indicates that this event was caused by an extreme EPB. Additionally, simultaneous and collocated GOLD observations confirm, unequivocally, that scintillations were caused by an extreme EPB. Moreover, GOLD provided information about the background F-region conditions under which the extreme EPBs and severe scintillation occurred. The observations are in good agreement with hypotheses about the ionospheric conditions favoring the rise of extreme EPBs put forward by previous studies (Mendillo et al. 2005; Krall et al. 2010).

Instrumentation and observations

As part of an ongoing experimental effort that seeks to better understand the occurrence and severity of ionospheric scintillation at mid-latitudes, ScintPi 3.0 (Gomez Socola and Rodrigues 2022) ionospheric monitors were deployed over Puerto Rico. ScintPi 3.0 may be described as an updated version of the ScintPi monitor presented by Rodrigues and Moraes (2019). Instead of a single-frequency Global Positioning System (GPS)-only receiver, however, ScintPi 3.0 uses a dual-frequency GNSS receiver. Consequently, ScintPi 3.0 measures the severity of ionospheric scintillation (S_4 index) at two frequencies (~1.2 and ~1.5 GHz) using signals transmitted by GPS, Globalnaya Navigazionnaya Sputnikovaya Sistema (GLONASS), Galileo, and Beidou. The dual-frequency measurements made by SciniPi 3.0 also allow the estimation of the ionospheric TEC. The S_4 index corresponds to the standard deviation of signal intensity normalized by its average (Briggs and Parkin 1963; Yeh and Liu 1982). ScintPi 3.0 monitors were installed at three different sites in Puerto Rico and started observations in December 2021. The location of the sites and relevant information are provided in Table 1.

A unique set of space-based observations complement ScintPi 3.0 measurements, providing information that was used to determine the origin of the TEC depletions

Table 1 Location of the ScintPi 3.0 monitors and relevant information

Station	Geog. Lat	Geog. Long	Dip latitude	Apex height
Culebra (Remote Facility—ROF) LT = UT-4.35	18.33°N	65.31°W	24.11°N	1880 km
Arecibo (Arecibo Observatory—AO) LT = UT-4.45	18.35°N	66.75°W	24.62°N	1950 km
Quebradillas (citizen science collaboration) LT = UT-4.46	18.47°N	66.91°W	24.78°N	1974 km

Apex height refers to the height at which the geomagnetic field line (at 350 km over each site) passes the magnetic equator

and scintillations observed over Puerto Rico. These observations were made by the NASA GOLD mission, which has a dual-channel ultraviolet-imaging spectrograph on SES-14, a communication satellite in geostationary orbit at 47.5°W longitude. The instrument makes measurements of the Earth far ultraviolet (FUV) airglow at ~134–162 nm. GOLD observations include images of the Earth sunlit and nightside disk, limb scans, and stellar occultations, from 06:10 UT up to 00:40 UT each day (Eastes et al. 2020). The nighttime scans cover about 45° in longitude and have a cadence of 15 min per scan.

In this study, the GOLD nighttime partial disk observations of the OI 135.6 nm emission, which serves as a proxy of ionospheric F-region densities, were employed. These observations have been used to track the behavior of the Equatorial Ionization Anomaly (EIA) and the occurrence of EPBs (Eastes et al. 2019; Aa et al. 2019). The observations made on the night of March 13–14, 2022, are analyzed and discussed in this study. During this night, large TEC depletions and severe scintillation events occurred at the latitudes of Puerto Rico and above.

Results and discussion

In this section, the results are summarized and discussed. First, the spatio-temporal evolution of ionospheric scintillation activity during the night of the event is presented. In the sequence, the severity of the TEC depletions, coincident with the occurrence of the scintillation in the signals, is analyzed. Subsequently, the GOLD observations are discussed, providing unequivocal evidence of the extreme EPB event as the source of the TEC depletions and ionospheric scintillation over dip latitudes >28°. In addition, a discussion on the conditions leading to this extreme EPB event is also presented.

On the spatio-temporal evolution of L-band scintillation

Figure 1 summarizes the observations made by the three ScintPi 3.0 receivers on March 13–14, 2022. It shows S_4 indices (see colorbar) for GNSS ~1.2 GHz signals in their corresponding Ionospheric Pierce Points (IPP) at 350 km altitude for sequential hours. Each panel exhibits the results for a time interval of 1 h during which observations were made. These time intervals are indicated in the respective left-bottom corners. Isolines of magnetic dip latitudes (magenta lines) and apex heights (black dashed lines) are also shown for reference. The dip latitudes and apex heights were computed from the International Geomagnetic Reference Field (IGRF13) model for March 2022. Computations considered the magnetic field lines starting points at the nominal F-region peak height (350 km), where irregularities contributing the most to scintillation are believed to be located.

The most striking result shown in Fig. 1 is the occurrence of strong scintillation ($S_4 > 0.9$ at 1.2 GHz) over Puerto Rico and at higher latitudes. The detection of this level of scintillation is unusual for mid-latitudes and is typically reported for observations made near the EIA peak, at lower latitudes. Figure 1 also serves to track the spatio-temporal evolution of the scintillation in the signals. The scintillation was first observed between 23:00 and 24:00 UT on March 13, 2022 at around 21° dip latitude, corresponding to regions with magnetic field lines reaching around 1400 km apex heights. By 01:00–02:00 UT, scintillation extended to higher latitudes and can be seen at dip latitudes >28°, i.e., where magnetic field line apex heights are >2600 km.

On the severity of scintillation and TEC conditions

Figure 1 already shows that moderate and intense scintillation could be observed in signals recorded by the ScintPi 3.0 monitors. Figure 2 better illustrates the severity of the observed scintillations and shows examples of TEC conditions under which these scintillation events occurred. The upper panels (a–c) show the relative slant TEC inferred from signals transmitted by GPS SVID 11 and measured by the ScintPi 3.0 receivers located at Culebra, Arecibo, and Quebradillas, from left to right, respectively. The middle panels (d–f) exhibit the S_4 indices for 1.2 (red) and 1.5 (black) GHz. The lower panel (g) shows the IPPs (at 350 km) of the signals for the three receiving stations. SVID stands for Space Vehicle Identification.

Note that Arecibo and Quebradillas are separated by only about 30 km and that the IPPs and measurements for these stations are very similar. As a result, the IPP tracks for these stations on panel (g) overlap. Culebra, however, is located about 200 km to the east of Arecibo, and the measurements are somewhat different. The measurements in the three sites, nevertheless, confirm that intense scintillation occurred in both frequencies. As expected from previous theoretical and experimental studies (Fremouw et al. 1978; Salles et al. 2021), scintillation on 1.2 GHz is stronger than scintillation on 1.5 GHz signals. This example shows S_4 at 1.2 GHz >0.8. More importantly, the observations serve to illustrate the finding that scintillations were accompanied by steep TEC variations that resemble those observed at lower latitudes during EPB events.

On simultaneous and collocated GOLD observations

The spatio-temporal behavior of the event detected on March 13–14, 2022, indicates that irregularities causing scintillation had origin at low latitudes. More specifically, the scintillations could have been caused by irregularities associated with EPBs. The TEC behavior that accompanied the scintillation reinforced the hypothesis that this

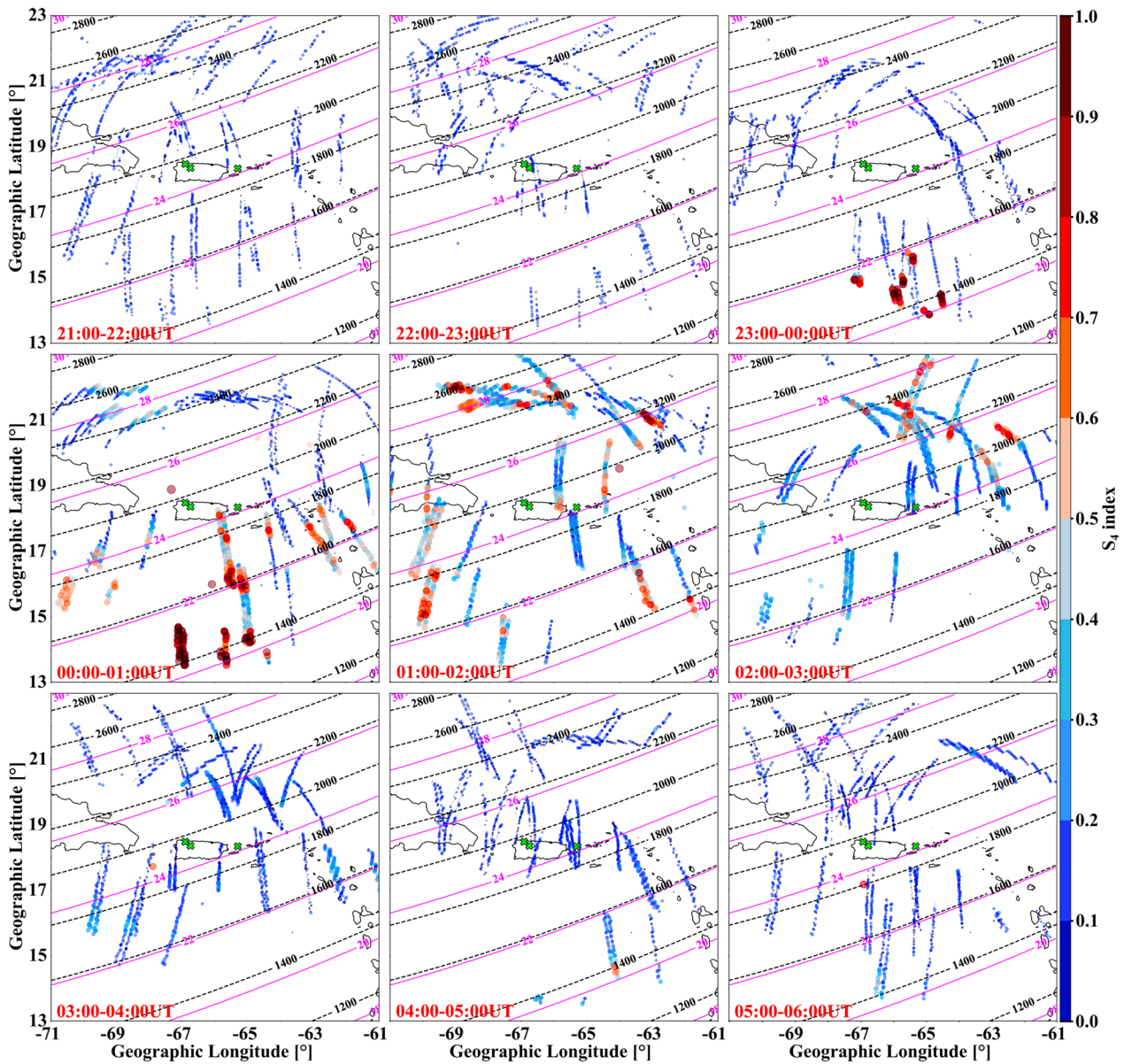


Fig. 1 S_4 indices for all the 1.2 GHz GNSS signals measured by the three ScintPi 3.0 receivers deployed over Puerto Rico. Each panel exhibits an 1-h frame during which observations were made. The time interval is indicated in the left-bottom corner of each panel. The green X markers indicate the location of the monitors. The solid magenta lines show dip latitudes ($^{\circ}$), and the dashed black lines indicate the corresponding equatorial apex heights (in km). The S_4 values are represented by colors according to the colormap on the right and by the size of the dots. Only data from satellites with elevation angles greater than 30° were used

mid-latitude scintillation was caused by EPBs reaching abnormally high apex heights (> 2600 km) and magnetic dip latitudes ($> 28^{\circ}$). Considering that scintillations were detected at dip latitudes corresponding to 1400 km apex heights at around 23:00 UT and at 2600 km apex heights at around 02:00 UT, one can estimate that an EPB would have to move vertically (over the equator) at approximately 111 m/s (on average). This vertical velocity is in

good agreement with expectations of EPB rising velocities (Abdu et al. 1983).

The deployment and observations provided by the ScintPi 3.0 monitors are timely as GOLD observations of the nighttime F-region ionosphere in the American sector are currently available. Most of the studies reporting the detection of extreme EPBs relied on ground-based measurements and, consequently, had limitations in either spatial resolution or coverage.

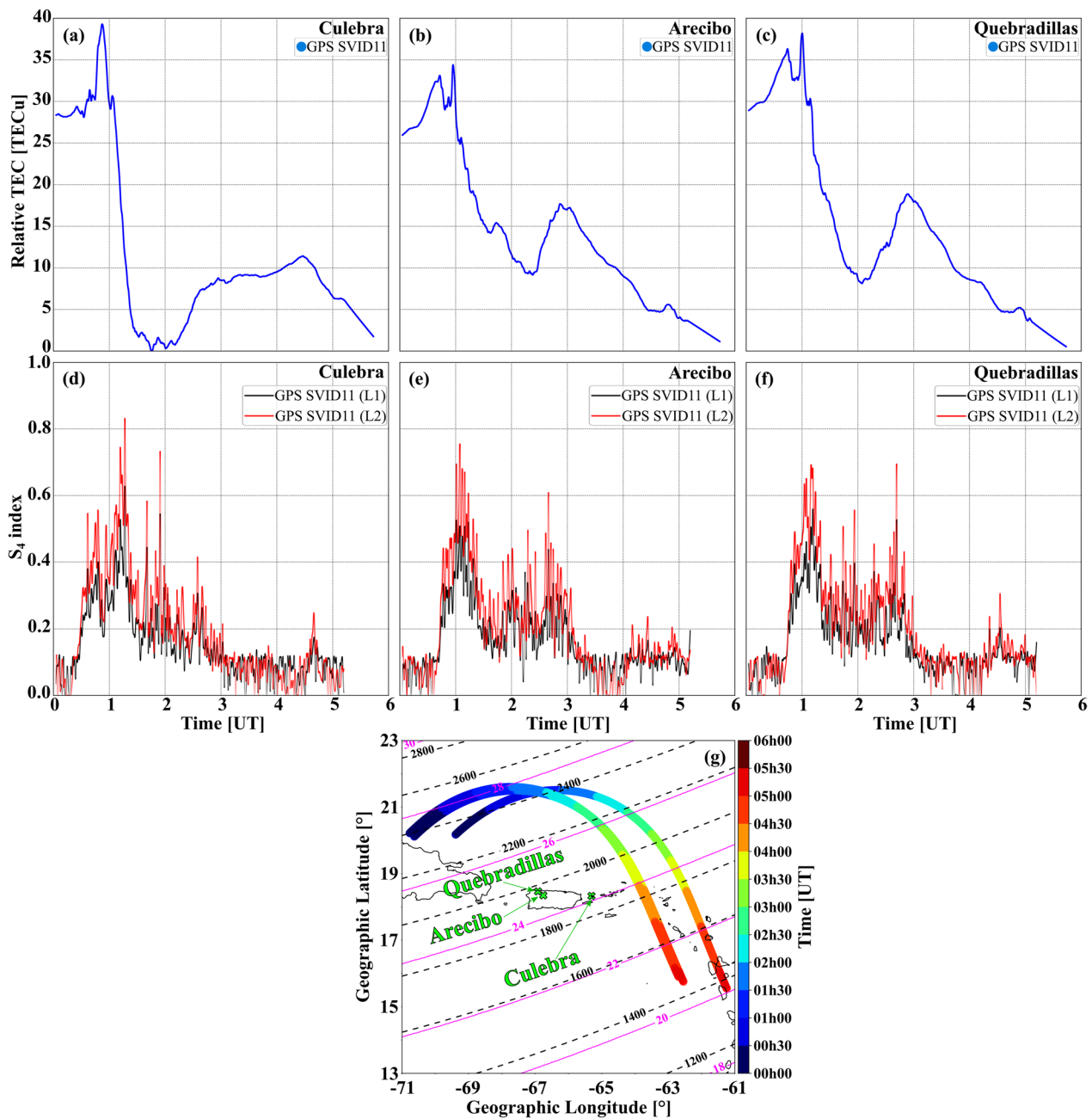


Fig. 2 TEC depletions and ionospheric scintillation recorded by the three ScintPi 3.0 stations over Puerto Rico. Upper panels (a–c): Steep TEC depletions (“bite-outs”) over Culobra, Arcibo, and Quebradillas. Middle panels (d–f): Strong ionospheric scintillation for the L1 (1.5 GHz) and L2 (1.2 GHz) signals transmitted by GPS SVID11 on March 13–14, 2022. Lower panel (g): IPPs of the signals from the GPS SVID11 for the three stations. Please notice that Arcibo and Quebradillas stations are close to each other and their IPPs overlap

Observations based on ground-based TEC receivers, for instance, had limitations due to the sparse distribution of sensors and a lack of measurements over the oceans. GOLD observations, as presented here, represent a new contribution in the detection and understanding of the extreme EPBs. GOLD images

are well-suited to aid the interpretation of the source of mid-latitude scintillation since its wide coverage over continents and oceans allows adequate comparison with the scintillation monitor observations.

The upper panels of Fig. 3 show a sequence of the OI 135 nm emission measurements made by GOLD between

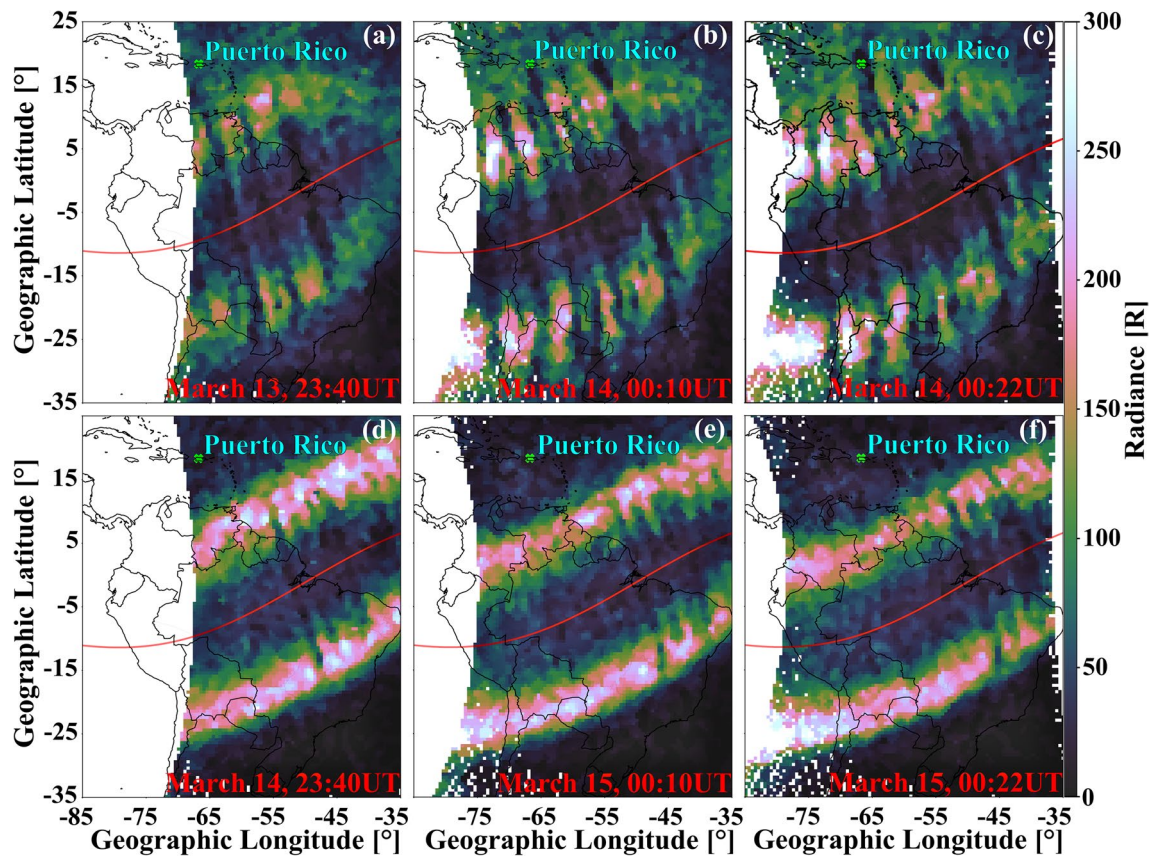


Fig. 3 Upper panels (a–c): OI 135 nm images measured by GOLD on March 13–14, 2022. The images exhibit extreme EPBs reaching latitudes larger than that of Puerto Rico (green X). Lower panels (d–f): OI 135 nm images measured by GOLD on March 14–15, 2022. The observations on March 14–15 are shown for comparison purposes and exhibit more typical latitudinal extents of the EIA and the EPBs

March 13 23:40 UT and March 14 00:22 UT. For comparison purposes, the lower panels show GOLD images for the following night (March 14–15, 2022). The solid red line indicates the location of the magnetic equator.

The images reveal regions of enhanced emission located at off-equator latitudes. These emissions indicate the location of the EIA peaks. The dark streaks of reduced emission nearly aligned with the magnetic meridian are signatures of EPBs. More importantly, the images reveal that, during the night of March 13–14, the EIA region was expanded to abnormally high latitudes. For reference, images for March 14–15 (lower panels) show an example of EIA that is representative of typical conditions, that is, with peaks that are more compact in latitude and closer to the magnetic equator. In addition to an expanded EIA, GOLD images reveal that EPBs reached abnormally high latitudes on March 13–14. For instance, the image on panel (a) shows the occurrence of enhanced background emissions (ionospheric densities) around Puerto Rico. In the sequence, at 00:10 UT and 00:22 UT of March 14, the images show EPBs above Puerto Rico and beyond, respectively. The enhanced background

F-region densities and the EPBs may also explain the severe L-band scintillation observed by the monitors over Puerto Rico (e.g., Basu et al. 1988). Enhanced background densities lead to density perturbations (Δn) with large amplitudes and, potentially, to more intense amplitude scintillation (Yeh and Liu 1982). More recent studies, however, pointed out that variations in the irregularity spectrum might also contribute to variations in the magnitude of L-band scintillation. Bhattacharyya et al. (2017, 2019) show that irregularities with a “shallow” spectrum would, in combination with a high ambient plasma density around the EIA, produce strong scintillation on the L-band. According to their results, this “shallow” spectrum would be more likely to be associated with topside EPBs. In the event discussed on this work both conditions are present, i.e., large ambient plasma density and EPBs reaching very high topside altitudes.

As mentioned earlier, GOLD images allow a more direct comparison between the scintillation measurements and the underlying F-region conditions. An example of such comparison is presented in Fig. 4, where scintillation measurements made within ± 10 min of the

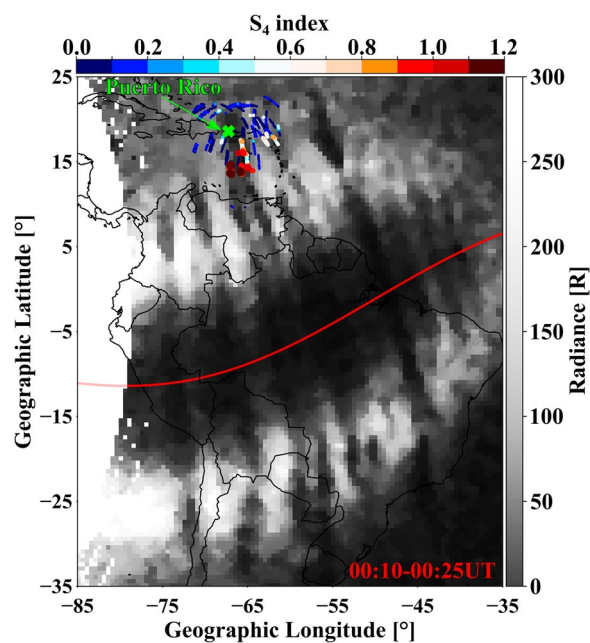


Fig. 4 Collocated GOLD OI 135 nm and ground-based scintillation observations made on March 14, 2022. GOLD images are for 00:10–00:25 UT. Scintillation measurements are for ± 10 min within the time of the GOLD image

GOLD image (00h10-00h25 UT) are exhibited. More specifically, Fig. 4 shows the S_4 values measured by the ScintPi 3.0 monitors overlaid on the GOLD OI 135 nm images. For this comparison OI emission intensities are represented by a grayscale colormap. The size and color of each scintillation value represented in the figure are related to its amplitude. It can be seen that regions of enhanced S_4 are well correlated with the EPBs (darkest bands) in the GOLD image. The comparison confirms, unambiguously, that the scintillation events were caused by extreme EPBs reaching the latitudes of Puerto Rico and beyond.

On the conditions leading to extreme EPBs

In the previous sections, new TEC and scintillation measurements made in Puerto Rico were presented and a unusual occurrence of an intense mid-latitude L-band scintillation event over dip latitudes $> 28^\circ$ was discussed. Using simultaneous and collocated GOLD images, it was possible to demonstrate that the scintillation events were caused by an extreme EPB. This section presents a possible explanation for the abnormally high rise of the EPBs observed on March 13–14, 2022.

The explanation follows the hypothesis put forward by Mendillo et al. (2005) and the numerical experiment presented by Krall et al. (2010). Mendillo et al. (2005) argued

that EPBs stop rising when the flux-tube integrated electron density inside the EPB matches the flux-tube integrated density of the surrounding background ionospheric plasma. Krall et al. (2010) evaluated this proposition using numerical simulations of EPBs performed by the Naval Research Laboratory SAMI3/ESF code (Huba et al. 2008) and found evidence supporting the Mendillo et al. (2005) hypothesis.

GOLD observations not only provide information about the occurrence and extent of EPBs, but also about the background F-region plasma conditions under which they appeared. On the night of March 13–14, 2022 the observations show an unusually wide EIA with the background density peaks extending to latitudes much higher than typically observed, especially over the northern hemisphere (please, compare GOLD observations for March 13–14 and March 14–15 in Fig. 3). The expanded EIA and large F-region electron densities at mid-latitudes on March 13–14 indicate height profiles of flux-tube integrated densities scale heights that are larger than those of most days. As a consequence, EPBs would have to rise to higher altitudes to reach a region where their internal flux-tube integrated density matches that of the background ionospheric plasma. Therefore, the observations indicate conditions favoring the abnormally high rise of EPBs, as proposed by Mendillo et al. (2005).

While the focus of this work is to present experimental evidence that extreme EPBs can cause scintillation over mid-latitudes and evaluate the F-region conditions favoring the high rise of the EPBs, some insight on the geospace conditions leading to the observed F-region morphology (i.e., the expanded EIA) is also offered. In that respect, it must be pointed out that a two-step magnetic storm (Kamide et al. 1998) was under development on March 13. Therefore, the expanded EIA occurred during a period that may be described as geomagnetically disturbed, when the low-latitude plasma transport might be enhanced. Figure 5 presents two panels with information about the interplanetary magnetic field (B_z), the SYM/H index, and the interplanetary electric field (E_y) for the period between March 12 and 15, 2022. Please observe that this figure is showing more days only to highlight the geomagnetic changes during the period of interest (March 13–14). The upper panel exhibits the interplanetary magnetic field (black) and the SYM/H (red). A sudden storm commencement, following a southward B_z turning, started around 12:00 on March 13. Subsequently, additional oscillations in B_z were followed by decreases in the SYM/H (increases in the ring current) reaching values around -114 nT, which, according to the “classic” definition (e.g., Sugiura and Chapman 1960; Loewe and Prölss 1997) indicate a strong storm.

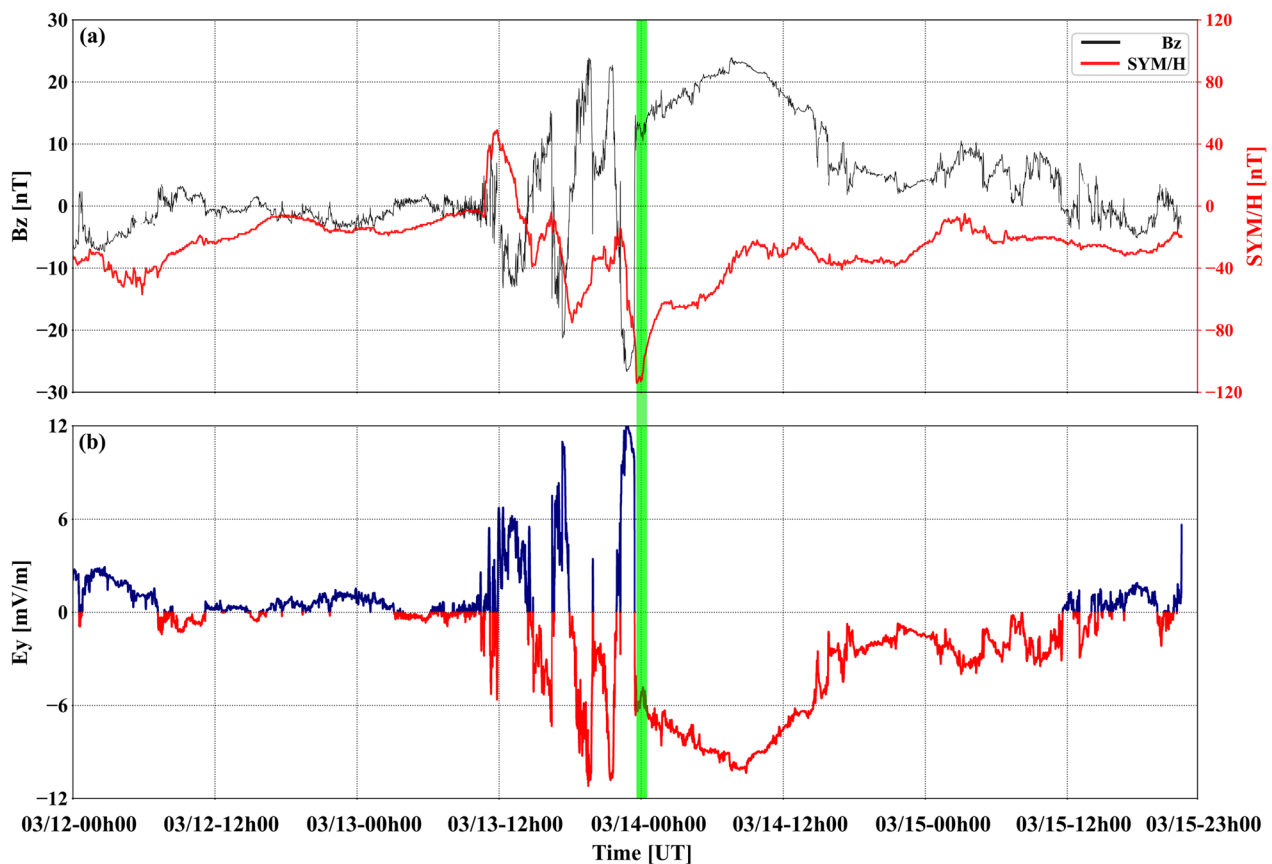


Fig. 5 Geomagnetic conditions over some days around the extreme EPB event. Upper panel: Interplanetary magnetic field (B_z) and SYM/H index revealing a storm onset around 12:00 UT on March 13. Lower panel: Interplanetary electric field (E_y) showing enhancements in magnitude during the geomagnetic storm period

The lower panel shows the interplanetary electric field (E_y) reaching magnitudes larger than 10 mV/m. Blue/red colors were used to indicate dawn-to-dusk/dusk-to-dawn orientation of the E_y . The green rectangular region corresponds to the interval of time presented in Fig. 4 (00:10–00:25 UT on March 14, 2022). Two mechanisms could have worked separately or conjointly, the disturbance dynamo (Blanc and Richmond 1980) and the disturbance electric fields (Senior and Blanc 1984).

Since the storm onset occurred several hours before the dusk, the disturbance dynamo effects had time to alter the equatorial electrodynamics, leading to an enhanced uplift of the plasma and contributing to the expansion of the EIA crests. However, an intense increase in E_y was noticed a few minutes before the extreme EPB event presented in Figs. 3 and 4 as well. According to Kelley et al. (2003), the “efficiency” of the so-called penetration electric field would be about $\sim 6.6\%$ of E_y . The E_y reached 12.21 mV/m at 22:49 UT on March 13, 2022, and, therefore, could have caused a penetration electric field of about 0.81 mV/m. If the magnetic field intensity at the

equatorial region corresponding to that magnetic field line apex is considered (20953 nT) and assuming a purely E/B vertical drift (i.e., no contribution from meridional winds), that would lead to an additional upward velocity of ~ 38.46 m/s. Therefore, penetration electric fields could also have been responsible for the enhanced redistribution of plasma to higher latitudes, leading to the expanded EIA observed on March 13–14, 2022. Rajesh et al. (2021) presented one example of such mid-latitude plasma density enhancement under the combination of geomagnetic storm induced neutral winds and increased fountain effect due to penetration electric fields action. Maruyama et al. (2005) used simulation to explore how the merged contribution from the disturbance dynamo and prompt penetration electric fields could potentially lead to increased eastward electric field in the dusk sector, therefore, causing more poleward EIA crests.

More specific discussions about the effects of geomagnetically disturbed conditions on the low and mid-latitudes can be found by Blanc and Richmond (1980), Abdu,

(1995, 1997, 2012), Kelley et al. (2003), Huang et al. (2007b), and Fejer et al. (2008, 2021).

Conclusion

Previous studies discussing the detection of ionospheric irregularities and/or scintillation events over mid-latitudes proposed distinct explanations for these events (e.g., Mendillo et al. 1997; Kelley, et al. 2000; Martinis et al. 2015; Kil et al. 2016; Hysell et al. 2016). Kil et al. (2016) pointed out that the observational gap in the region between equatorial and mid-latitudes could be one of the main obstacles for a more conclusive determination of the sources of irregularities and scintillation observed at mid-latitudes.

This work presents new joint ground- and space-based observations showing unequivocal evidence of severe L-band ionospheric scintillations and large TEC depletions over low-to-mid latitudes caused by extreme EPBs, that is, EPBs reaching extremely high magnetic apex heights.

Measurements made by ground-based ionospheric scintillation and TEC monitors deployed in Puerto Rico provided information indicating that ionospheric irregularities and scintillation originated at low latitudes and propagated, subsequently, to mid-latitudes. Simultaneous imaging of the ionospheric F-region from equatorial to mid-latitudes provided by the GOLD mission confirmed, conclusively, that the ionospheric irregularities and scintillation observed over Puerto Rico and higher latitudes were indeed caused by extreme EPBs. These observations are in good agreement with previously proposed theories and numerical simulations. The ground-based and satellite measurements show that plasma bubbles reached apex heights exceeding 2600 km and magnetic dip latitudes beyond 28°. GOLD observations also reveal an abnormal expansion (in latitude) of the EIA. Finally, GOLD shows enhanced background F-region densities at mid-latitudes favoring the occurrence of intense L-band scintillation when topside EPBs reach that region.

Acknowledgements

The Arecibo Observatory is operated by the University of Central Florida under a cooperative agreement with the National Science Foundation (AST-1744119) and in alliance with Yang Enterprises and Ana G. Méndez-Universidad Metropolitana. CGMB and PT would like to thank the support from NSF Award AGS-2221770. RWE and GOLD mission are supported by NASA contract 80GSFC18C0061 to the University of Colorado. The authors greatly acknowledge Mr. Carlos Pérez for hosting the ScintiPi 3.0 deployed at Quebradillas.

Author contributions

JSS and FSR conceived the work. JSS performed the data analysis and interpretation, produced the figures and wrote the manuscript. FSR contributed to interpretation of the results and writing of the manuscript. JGS carried out the development and data processing from the ScintiPi monitors. RWE provided the GOLD data and contributed to the writing of the manuscript. CGMB and PT contributed to make the ScintiPi measurements over Puerto Rico possible

and also participated in the writing of the manuscript. All the authors read and approved the final manuscript.

Funding

Research at UT Dallas is supported by NSF awards AGS-1916055 and AGS-2122639.

Availability of data and materials

The GOLD data are available at GOLD Science Data Center (<https://gold.cs.ucf.edu/data/search/>) and at NASA's Space Physics Data Facility (<http://spdf.gsfc.nasa.gov/>). Geomagnetic indices may be accessed at https://omniweb.gsfc.nasa.gov/form/omni_min.html. Ionospheric scintillation and TEC data used in this study can be accessed at <https://zenodo.org/record/7734875>.

Declarations

Competing interests

The authors declare that they have no competing interests.

Author details

¹William B. Hanson Center for Space Sciences, University of Texas at Dallas, Richardson, TX, USA. ²Laboratory for Atmospheric and Space Physics, University of Colorado Boulder, Boulder, CO, USA. ³Arecibo Observatory, Puerto Rico, USA.

Received: 7 November 2022 Accepted: 3 March 2023

Published online: 21 March 2023

References

- Aa E, Huang W, Liu S, Ridley A, Zou S, Shi L, Chen Y, Shen H, Yuan T, Li J, Wang T (2018) Midlatitude plasma bubbles over China and adjacent areas during a magnetic storm on 8 September 2017. *Space Weather* 16(3):321–331. <https://doi.org/10.1002/2017SW001776>
- Aa E, Zhou S, Eastes RW, Karan DK, Zhang SR, Erickson P, Coster AJ (2019) Coordinated ground-based and space-based observations of equatorial plasma bubbles. *J Geophys Res* 125(1):1–13. <https://doi.org/10.1029/2019JA027569>
- Aa E, Zhang SR, Erickson PJ, Vierinen J, Coster AJ, Goncharenko LP (2022a) Significant ionospheric hole and equatorial plasma bubbles after the 2022a Tonga volcano eruption. *Space Weather*. <https://doi.org/10.1029/2022SW003101>
- Abdu MA (1997) Major phenomena of the equatorial ionosphere-thermosphere system under disturbed conditions. *J Atmos Solar Terr Phys* 59(13):1505–1519. [https://doi.org/10.1016/S1364-6826\(96\)00152-6](https://doi.org/10.1016/S1364-6826(96)00152-6)
- Abdu MA (2012) Equatorial spread F/plasma bubble irregularities under storm time disturbance electric fields. *J Atmos Solar Terr Phys* 75–76:44–56. <https://doi.org/10.1016/j.jastp.2011.04.024>
- Abdu MA, de Medeiros RT, Bittencourt JA, Batista IS (1983) Vertical ionization drift velocities and range type spread F in the evening equatorial ionosphere. *J Geophys Res* 88(A1):399–402. <https://doi.org/10.1029/JA088iA01p00399>
- Abdu MA, Batista IS, Walker GO, Sobral JHA, Trivedi NB, de Paula ER (1995) Equatorial ionospheric electric fields during magnetospheric disturbances: local time/longitude dependences from recent EITS campaigns. *J Atmos Terr Phys* 57(10):1065–1083. [https://doi.org/10.1016/0021-9169\(94\)00123-6](https://doi.org/10.1016/0021-9169(94)00123-6)
- Basu S, Basu S, Khan K (1976) Model of equatorial scintillations from in-situ measurements. *Radio Sci* 11(10):821–832. <https://doi.org/10.1029/RS011i010p00821>
- Basu S, MacKenzie E, Basu S (1988) Ionospheric constraints on VHF/UHF communications links during solar maximum and minimum periods. *Radio Sci* 23(3):363–378. <https://doi.org/10.1029/RS023i003p00363>
- Basu S, Basu S, Groves KM, MacKenzie E, Keskinen MJ, Rich FJ (2005) Near-simultaneous plasma structuring in the midlatitude and equatorial ionosphere during magnetic superstorms. *Geophys Res Lett* 32(12):1–4. <https://doi.org/10.1029/2004GL021678>
- Basu S, Basu S, Rich FJ, Groves KM, MacKenzie E, Coker C, Sahai Y, Fagundes PR, Guedes FB (2007) Response of the equatorial ionosphere at dusk to

- penetration electric fields during intense magnetic storms. *J Geophys Res Space Phys* 112(A8):1–14. <https://doi.org/10.1029/2006JA012192>
- Beach T, Kintner PM (2001) Development and use of a GPS ionospheric scintillation monitor. *IEEE Trans Geosci Remote Sens* 39(5):918–928. <https://doi.org/10.1109/36.921409>
- Bhattacharyya A, Kakad B, Gurram P, Sripathi S, Sunda S (2017) Development of intermediate-scale structure at different altitudes within an equatorial plasma bubble: Implications for L-bad scintillations. *J Geophys Res Space Phys* 122(1):1015–1030. <https://doi.org/10.1002/2016JA023478>
- Bhattacharyya A, Gurram P, Kakad B, Sripathi S, Sunda S (2019) Signal frequency dependence of ionospheric scintillations: an indicator of irregularity spectrum characteristics. *J Geophys Res Space Phys* 124(10):8081–8091. <https://doi.org/10.1029/2019JA026987>
- Blanc M, Richmond AD (1980) The ionospheric disturbance dynamo. *J Geophys Res Space Physics* 85(A4):1669–1686. <https://doi.org/10.1029/JA085iA04p01669>
- Briggs BH, Parkin IA (1963) On the variation of radio star and satellite scintillations with zenith angle. *J Atmos Terr Phys* 25(6):339–366. [https://doi.org/10.1016/0021-9169\(63\)90150-8](https://doi.org/10.1016/0021-9169(63)90150-8)
- Carrano CS, Delay S, Pradipta R, Groves KM, Doherty PH. (2021). Rates of cycle slips and outages for GPS L1/L2C/L5 due to ionospheric scintillation. Proceedings of the 34th International Technical Meeting of the Satellite Division of The Institute of Navigation (ION GNSS+ 2021), St. Louis, Missouri, September 2021, p. 3897–3909, doi: <https://doi.org/10.33012/2021.18060>
- Chapagain NP, Fejer BG, Chau JL (2009) Climatology of postsunset equatorial spread F over Jicamarca. *J Geophys Res Space Physics* 114(A7):1–7. <https://doi.org/10.1029/2008JA013911>
- Cherniak I, Zakharenkova I (2016) First observations of siper plasma bubbles in Europe. *Geophys Res Lett* 43(21):11137–11145. <https://doi.org/10.1002/2016GL071421>
- Cherniak I, Zakharenkova I (2022) Development of the storm-induced ionospheric irregularities at equatorial and middle latitudes during the 25–26 august 2018 geomagnetic storm. *Space Weather* 20(2):1–18. <https://doi.org/10.1029/2021SW002891>
- Eastes RW, Solomon SC, Daniell RE, Anderson DN, Burns AG, England SL, Martinis CR, McClintock WE (2019) Global-scale observations of the equatorial ionization anomaly. *Geophys Res Lett* 46(16):9318–9326. <https://doi.org/10.1029/2019GL084199>
- Eastes RW, McClintock WE, Burns AG, Anderson DN, Andersson L, Aryal S, Budzien SA, Cai X, Codrescu MV, Correira JT, Daniell RE, Dymond KF, England SL, Eparvier FG, Evans JS, Foroosh H, Gan Q, Greer KR, Karan DK, Krywonos A, Laskar FI, Lumpe JD, Martinis CR, McPhate JB, Oberheide J, Siegmund OH, Solomon SC, Veibel V, Woods TN (2020) Initial observations by the GOLD mission. *J Geophys Res Space Phys* 125:1–11. <https://doi.org/10.1029/2020JA027823>
- Fejer BG, Jensen JW, Su SY (2008) Seasonal and longitudinal dependence of equatorial disturbance vertical plasma drifts. *Geophys Res Lett* 35(L20106):1–4. <https://doi.org/10.1029/2008GL035584>
- Fejer BG, Navarro LA, Sazykin S, Newheart A, Milla MA, Condor P (2021) Prompt penetration and substorm effects over Jicamarca during the september 2017 geomagnetic storm. *J Geophys Res Space Phys* 126(8):1–11. <https://doi.org/10.1029/2021JA029651>
- Fernandez L, Ruiz-de-Azua JA, Calveras A, Camps A (2020) Assessing LoRa for satellite-to-Earth communications considering the impact of ionospheric scintillation. *IEEE Access* 8:165570–165582. <https://doi.org/10.1109/ACCESS.2020.3022433>
- Fremouw EJ, Leadabrand RL, Livingston RC, Cousins MD, Rino CL, Fair BC, Long RA (1978) Early results from the DNA Wideband satellite experiment-Complex-signal scintillation. *Radio Sci* 13(1):167–187. <https://doi.org/10.1029/RS013i001p0167>
- Gomez Socola J, Rodrigues FS (2022b) ScintPi 2.0 and 3.0: low-cost GNSS-based monitors of ionospheric scintillation and total electron content. *Earth Planets Space* 74(185):1–18. <https://doi.org/10.1186/s40623-022-01743-x>
- Haerendel G, Eccles JV, Çakir S (1992) Theory for modeling the equatorial evening ionosphere and the origin of the shear in the horizontal plasma flow. *J Geophys Res Space Phys* 97(A2):1209–1223. <https://doi.org/10.1029/91JA02226>
- Huang CS, Foster JC, Sahai Y (2007a) Significant depletions of the ionospheric plasma density at middle latitudes: a possible signature of equatorial spread F bubbles near the plasmopause. *J Geophys Res Space Phys* 112(A5):1–13. <https://doi.org/10.1029/2007JA012307>
- Huang CS, Sazykin S, Chau JL, Maruyama N, Kelley MC (2007b) Penetration electric fields: efficiency and characteristic time scale. *J Atmos Solar Terr Phys* 69(10–11):1135–1146. <https://doi.org/10.1016/j.jastp.2006.08.016>
- Huba JD, Joyce G, Krall J (2008) Three-dimensional equatorial spread F modeling. *Geophys Res Lett* 35(10):1–5. <https://doi.org/10.1029/2008GL033509>
- Hysell DL, Larsen M, Sulzer M (2016) Observational evidence for new instabilities in the midlatitude E and F region. *Ann Geophys* 34:927–941. <https://doi.org/10.5194/angeo-34-927-2016>
- Jiao Y, Morton YT (2015) Comparison of the effect of high-latitude and equatorial ionospheric scintillation on GPS signals during the maximum of solar cycle 24. *Radio Sci* 50(9):886–903. <https://doi.org/10.1002/2015RS005719>
- Juan JM, Sanz J, González-Casado G, Rovira-García A, Camps A, Riba J, Barbosa J, Blanch E, Altadill D, Perez RO (2018) Feasibility of precise navigation in high and low latitude regions under scintillation conditions. *J Space Weather Space Climate* 8(A05):1–11. <https://doi.org/10.1051/swsc/2017047>
- Kamide Y, Yokoyama N, Gonzalez W, Tsurutani B, Dagis IA, Brekke A, Masuda S (1998) Two-step development of geomagnetic storms. *J Geophys Res Space Phys* 103(A4):6917–6921. <https://doi.org/10.1029/97JA03337>
- Katamzi-Joseph ZT, Habarulema JB, Hernández-Pajares M (2017) Midlatitude postsunset plasma bubbles observed over Europe during intense storms in April 2000 and 2001. *Space Weather* 15(9):1177–1190. <https://doi.org/10.1002/2017SW001674>
- Kelley MC, Garcia F, Makela JJ, Fan T, Mak E, Sia C, Alcocer D (2000) Highly structured tropical airglow and TEC signatures during strong geomagnetic activity. *Geophys Res Lett* 27(4):465–468. <https://doi.org/10.1029/1999GL000598>
- Kelley MC, Makela JJ, Chau JL, Nicolls MJ (2003) Penetration of the solar wind electric field into the magnetosphere/ionosphere system. *Geophys Res Lett* 30(4):1–3. <https://doi.org/10.1029/2002GL016321>
- Kelly MA, Comberiate JM, Miller ES, Paxton LJ (2014) Progress toward forecasting of space weather effects on UHF SATCOM after Operation Anaconda. *Space Weather* 12(10):601–661. <https://doi.org/10.1002/2014SW001081>
- Kill H, Miller ES, Jee G, Kwak YS, Zhang Y, Nishioka M (2016) Comment on “The night when the auroral and equatorial ionospheres converged.” *J Geophys Res Space Phys* 121(10):10599–10607. <https://doi.org/10.1002/2016JA022662>
- Krall J, Huba JD, Ossakow SL, Joyce G (2010) Why do equatorial ionospheric bubbles stop rise? *Geophys Res Lett* 37(L09105):1–4. <https://doi.org/10.1029/2010GL043128>
- Li G, Ning B, Wang C, Abdu MA, Otsuka Y, Yamamoto M, Wu J, Chen J (2018) Storm-enhanced development of postsunset equatorial plasma bubbles around the meridian 120°E/60°W on 7–8 September 2017. *J Geophys Res Space Phys* 123(9):7985–7998. <https://doi.org/10.1029/2018JA025871>
- Loewe CA, Prölsch GW (1997) Classification and mean behavior of geomagnetic storms. *J Geophys Res Space Phys* 102(A7):14209–14213. <https://doi.org/10.1029/96JA04020>
- Ma G, Maruyama T (2006) A super bubble detected by dense GPS network at east Asian longitudes. *Geophys Res Lett* 33(21):1–5. <https://doi.org/10.1029/2006GL027512>
- Martinis C, Mendillo M (2007) Equatorial spread F-related airglow depletions at Arecibo and conjugate observations. *J Geophys Res Space Physics* 112(A12):1–9. <https://doi.org/10.1029/2007JA012403>
- Martinis C, Baumgardner J, Mendillo M, Su SY, Aponte N (2009) Brightening of 630.0 nm equatorial spread-F airglow depletions. *J Geophys Res Space Phys*. <https://doi.org/10.1029/2008JA013931>
- Martinis C, Baumgardner J, Wroten J, Mendillo M (2010) Seasonal dependence of MSTIDs obtained from 630.0 nm airglow imaging at Arecibo. *Geophys Res Lett*. <https://doi.org/10.1029/2010GL043569>
- Martinis C, Baumgardner J, Mendillo M, Wroten J, Coster A, Paxton L (2015) The night when the auroral and equatorial ionospheres converged. *J Geophys Res Space Physics* 120(9):8085–8095. <https://doi.org/10.1002/2015JA021555>
- Maruyama N, Richmond AD, Fuller-Rowell TJ, Codrescu MV, Sazykin S, Tof-foletto FR, Spiro RW, Millward GH (2005) Interaction between direct penetration and disturbance dynamo electric fields in the storm-time

- equatorial ionosphere. *Geophys Res Lett* 32(17):L17105. <https://doi.org/10.1029/2005GL023763>
- Mathews JD, Machuga DW, Zhou Q (2001a) Evidence for electrodynamic linkages between spread-F, ion rain, the intermediate layer, and sporadic E: results from observations and simulations. *J Atmos Solar Terr Phys* 63(14):1529–1543. [https://doi.org/10.1016/S1364-6826\(01\)00034-7](https://doi.org/10.1016/S1364-6826(01)00034-7)
- Mathews JD, González S, Sulzer MP, Zhou QH, Urbina J, Kudeki E, Franke S (2001b) Kilometer-scale layered structures inside spread-F. *Geophys Res Lett* 28(22):4167–4170. <https://doi.org/10.1029/2001GL013077>
- Mendillo M, Baumgardner J, Nottingham D, Aarons J, Reinisch B, Scali J, Kelley MC (1997) Investigations of thermospheric-ionospheric dynamics with 6300-Å images from the Arecibo observatory. *J Geophys Res Space Phys* 102(A4):7331–7343. <https://doi.org/10.1029/96JA02786>
- Mendillo M, Zesta E, Shodhan S, Sultan PJ, Doe R, Sahai Y, Baumgardner J (2005) Observations and modeling of the coupled latitude-altitude patterns of equatorial plasma depletions. *J Geophys Res Space Phys* 110(A09303):1–7. <https://doi.org/10.1029/2005JA011157>
- Moraes AO, Vani BC, Costa E, Sousasantos J, Abdu MA, Rodrigues FS, Gladek YC, de Oliveira CBA, Monico JFG (2018) Ionospheric scintillation fading coefficients for the GPS L1, L2 and L5 frequencies. *Radio Sci* 53(9):1165–1174. <https://doi.org/10.1029/2018RS006653>
- Portella IG, Moraes AO, Pinho MS, Sousasantos J, Rodrigues FS (2021) Examining the tolerance of GNSS receiver phase tracking loop under the effects of severe ionospheric scintillation conditions based on its bandwidth. *Radio Sci* 56(6):1–11. <https://doi.org/10.1029/2020RS007160>
- Rajesh PK, Lin CH, Lin CY, Chen CH, Liu JY, Matsuo T, Chen SP, Yeh WH, Huang CY (2021) Extreme positive ionosphere storm triggered by a minor magnetic storm in deep solar minimum revealed by FORMOSAT-7/COSMIC-2 and GNSS observations. *J Geophys Res Space Phys*. <https://doi.org/10.1029/2020JA028261>
- Rajesh PK, Lin CCH, Lin JT, Lin CY, Liu JY, Matsuo T, Huang CY, Chou MY, Yue J, Nishioka M, Jin H, Choi JM, Chen SP, Chou M, Tsai HF (2022) Extreme poleward expanding super plasma bubbles over Asia-Pacific region triggered by Tonga volcano eruption during the recovery-phase of geomagnetic storm. *Geophys Res Lett*. <https://doi.org/10.1029/2022GL099798>
- Rodrigues FS, Moraes AO (2019) ScintPi: a low-cost, easy-to-build GPS ionospheric scintillation monitor for DASI studies of space weather, education, and citizen science initiatives. *Earth and Space Science* 6(8):1547–1560. <https://doi.org/10.1029/2019EA000588>
- Rodrigues FS, Socola JG, Moraes AO, Martinis C, Hickey DA (2021) On the properties of and ionospheric conditions associated with a mid-latitude scintillation event observed over southern United States. *Space Weather* 19(6):1–20. <https://doi.org/10.1029/2021SW002744>
- Salles LA, Moraes AO, Vani BC, Sousasantos J, Affonso BJ, Monico JFG (2021) A deep fading assessment of the modernized L2C and L5 signals for low-latitude regions. *GPS Solu* 25(122):1–13. <https://doi.org/10.1007/s10291-021-01157-4>
- Senior C, Blanc M (1984) On the control of magnetospheric convection by the spatial distribution of ionospheric conductivities. *J Geophys Res Space Phys* 89(1):261–284. <https://doi.org/10.1029/JA089iA01p00261>
- Sobral JHA, Abdu MA, Takahashi H, Taylor MJ, de Paula ER, Zamlutti CJ, Aquino MG, Borba GL (2002) Ionospheric plasma bubble climatology over Brazil based on 22 years (1977–1998) of 630nm airglow observations. *J Atmos Solar Terr Phys* 64(12–14):1517–1524. [https://doi.org/10.1016/S1364-6826\(02\)00089-5](https://doi.org/10.1016/S1364-6826(02)00089-5)
- Sori T, Otsuka Y, Shinbori A, Nishioka M, Perwitasari S (2022) Geomagnetic conjugacy of plasma bubbles extending to mid-latitudes during a geomagnetic storm on March 1, 2013. *Earth Plan Space* 74(120):1–16. <https://doi.org/10.1186/s40623-022-01682-7>
- Sousasantos J, Affonso BJ, Moraes AO, Rodrigues FS, Abdu MA, Salles LA, Vani BC (2022c) Amplitude scintillation severity and fading profiles under alignment between GPS propagation paths and equatorial plasma bubbles. *Space Weather*. <https://doi.org/10.1029/2022SW003243>
- Sugiura M, Chapman S. (1960). The average morphology of geomagnetic storms with sudden commencement. *Abhandl. Akad. Wiss. Göttingen, Math.-Phys. Kl., Sonderheft 4, Göttingen*
- Woodman RF, La Hoz C (1976) Radar observations of F region equatorial irregularities. *J Geophys Res Space Phys* 81(31):5447–5466. <https://doi.org/10.1029/JA081i031p05447>
- Yeh KC, Liu CH (1982) Radio wave scintillations in the ionosphere. *Proc IEEE* 70(4):324–360. <https://doi.org/10.1109/PROC.1982.12313>
- Zakharenkova I, Cherniak I (2020) When plasma streams tie up equatorial plasma irregularities with auroral ones. *Space Weather* 18(2):1–19. <https://doi.org/10.1029/2019SW002375>
- Zakharenkova I, Cherniak I (2021) Effects of storm-induced equatorial plasma bubbles on GPS-based kinematic positioning at equatorial and middle latitudes during the September 7–8, 2017, geomagnetic storm. *GPS Solutions* 25(132):1–14. <https://doi.org/10.1007/s10291-021-01166-3>

Publisher's Note

Springer Nature remains neutral with regard to jurisdictional claims in published maps and institutional affiliations.

Submit your manuscript to a SpringerOpen® journal and benefit from:

- Convenient online submission
- Rigorous peer review
- Open access: articles freely available online
- High visibility within the field
- Retaining the copyright to your article

Submit your next manuscript at ► [springeropen.com](https://www.springeropen.com)